Toward a consistent calculation of the lunar response to gravitational waves

Han Yan,[1,2] Xian Chen,[1,2,*] Jinhai Zhang,[3] Fan Zhang,[4,5] Mengyao Wang,[5] and Lijing Shao[2]

[1]*Department of Astronomy, School of Physics, Peking University, 100871 Beijing, China*
[2]*Kavli Institute for Astronomy and Astrophysics at Peking University, 100871 Beijing, China*
[3]*Institute of Geology and Geophysics, Chinese Academy of Sciences, Beijing 100029, China*
[4]*Institute for Frontiers in Astronomy and Astrophysics, Beijing Normal University, Beijing 102206, China*
[5]*Department of Astronomy, Beijing Normal University, Beijing 100875, China*

(Received 29 January 2024; accepted 13 March 2024; published 29 March 2024)

The recent increasing interest in detecting gravitational waves (GWs) by lunar seismic measurement urges us to have a clear understanding of the response of the moon to passing GWs. In this paper, we clarify the relationship between two seemingly different response functions which have been derived previously using two different methods, one taking the field-theory approach and the other using the tidal force induced by GWs. We revisit their derivation and prove, by both analytical arguments and numerical calculations, that the two response functions are equivalent. Their apparent difference can be attributed to the choice of different coordinates. Using the correct response function, we calculate the sensitivities (to GWs) of several designed lunar seismometers, and find that the sensitivity curves between 10^{-3} and 0.1 Hz are much flatter than the previous calculations based on normal-mode model. Our results will help clarify the scientific objectives of lunar GW observation, as well as provide important constraints on the design of lunar GW detectors.

DOI: 10.1103/PhysRevD.109.064092

I. INTRODUCTION

The detection of gravitational waves (GWs) in the frequency window of 10–10^2 Hz [1] as well as nano-Hz [2–5] encourages the efforts to detect GWs in other frequency bands. Several projects plan on using interferometers to detect millihertz (mHz) GWs, including the Laser Interferometer Space Antenna (LISA [6]), TianQin [7], and Taiji [8]. There are also discussions and designs of interferometers to probe deci-Hertz (0.1 Hz, or deci-Hz) GWs [9], such as the DECIGO [10] and TVLBAI [11].

An alternative approach is to take advantage of the quietness of the moon and use it as a resonant GW detector [12]. However, detecting the response of the moon to passing GWs requires a redesign of lunar seismometers, so as to achieve particularly high sensitivities. The recent studies based on several designs suggest that the sensitivity to GWs is the best around deci-Hz, which will allow us to detect merging white dwarf binaries, intermediate-mass black hole binaries (IMBHBs), and supermassive black hole binaries (SMBHBs) out to cosmological distances, as well as the GW background produced in the early universe [13,14].

One essential element in studying the lunar response to GW is the calculation of the force density imposed by GW on an elastic body. The theory was first laid down by Dyson ([15], hereafter Dy69). He started from the field theory and, by introducing a coupling term between GW and the elastic body, derived an external-force density

$$\vec{f} = -\nabla \cdot (\mu \mathbf{h}),$$

where μ is the shear modulus and $\mathbf{h}$ refers to the three-dimensional spatial components of the GW tensor. Using this equation, Dyson studied the response of an infinite half-space to a train of passing GW. Later, Ben-Menahem applied the same force density to a more realistic lunar model, a radially heterogeneous elastic sphere, and derived an analytical response solution ([16], hereafter BM83). A modern version of the derivation can be found in Ref. [17] (hereafter Ma19). These formulas derived in Dy69 and Ma19 form the basis for many later calculations of the lunar or Earth response to GWs [18–21]. They have also heavily influenced the scientific objectives of more recent lunar GW projects, including the Lunar GW Antenna (LGWA [13,22]).

An ambiguity, however, appears when one takes another viewpoint to calculate the lunar response function. In the early studies of ground-based bar detectors [23–27], it was common to write the force density due to GW in the form of

$$\vec{f} = \frac{1}{2}\rho \frac{\mathrm{d}^2 \mathbf{h}}{\mathrm{d}t^2} \cdot \vec{r},$$

where ρ is the mass density and $\vec{r}$ is the position vector. This formula is usually called the "tidal acceleration formula,"

*Corresponding author: xian.chen@pku.edu.cn

and has been adopted by many textbooks (e.g., [28,29]). It was also used in the recent science studies of lunar seismometer projects [14]. The apparent difference of this equation with respect to the previous one naturally raises the question about which force density should be used in the calculation of the lunar response.

This ambiguity has been noticed in several earlier papers. In his attempt to develop a fully general-relativistic treatment of the lunar response [30], Dozmorov noticed the difference between the two force densities [31]. He attributed the difference to two kinds of shear waves, one propagating at the speed of light and the other at the speed of seismic wave. However, he did not give further explanation to the cause or the relationship between these two waves. A recent review article [32] (hereafter Ha19) also discusses the physical meanings of the Dyson force and the tidal force by comparing the surface displacement computed with Newtonian mechanics and the displacement measured by an inertial sensor. It argues that the two displacements are equivalent, which hints that the two displacements are connected by a change of the coordinate system, but a quantitative proof is still lacking. Probably because of the inconclusiveness of the previous discussions, later works sometimes considered both types of forces and presented two response functions.

Inspired by these previous discussions, we decide to revisit the relevant theories and try to resolve the apparent inconsistency caused by the aforementioned two kinds of force densities. The paper is organized as follows. In Sec. II, we review the dynamical equations of an elastic body which is subject to the Dyson force or the tidal force, where we focus on clarifying the physical difference between the coordinate systems in which the equations are derived. We then derive two response functions, corresponding to the above two kinds of forces, and show that they can be unified into one analytical formula. In Sec. III, we apply our response functions to a homogeneous isotropic sphere and a real lunar model, to show that in both cases the numerical results agree with the analytical relationship. We also discuss the observability of GWs based on the appropriate response function. Finally, in Sec. IV, we summarize our results and discuss their implications for future lunar GW observation. Throughout the paper we will adopt the International System of Units and the Minkowski metric $\eta_{\mu\nu} = \mathrm{diag}(-1, 1, 1, 1)$, unless otherwise mentioned. Latin alphabets represent three spatial indices, and Greek alphabets represent spacetime indices.

II. THEORY

This section reviews the dynamical equation of an elastic system in a GW field with a flat spacetime background. Two sets of equations have been derived in the literature due to different viewpoints, one based on the transverse-traceless (TT) coordinate and the other in the lab frame. We will first review the derivation of the equations, then clarify their mathematical relation in the example of a radially heterogeneous elastic sphere.

A. Equations in the TT coordinate

When dealing with free particles moving in a GW field, it is normally convenient to use the TT coordinate. In this coordinate system, which we denote by the subscript A, the line element reads

$$\mathrm{d}s^2 = (\eta_{\mu\nu} + h^{\mathrm{TT}}_{\mu\nu})\mathrm{d}x^\mu_A \mathrm{d}x^\nu_A. \tag{1}$$

Hereafter, for simplicity, we will omit the superscript TT of the GW tensor $h_{\mu\nu}$. The corresponding geodesic equation of a free, slowly moving particle is

$$\frac{\mathrm{d}^2 x^i_A}{\mathrm{d}t^2} = 0, \tag{2}$$

where $i = 1, 2, 3$ denotes the three spatial directions. In this equation, $h_{\mu\nu}$ does not appear, verifying the convenience of using the TT coordinate. If, in addition, an electromagnetic (EM) force $f^i_{\mathrm{EM},A}$ is imposed on this particle, the equations of motion become

$$m\frac{\mathrm{d}^2 x^i_A}{\mathrm{d}t^2} = f^i_{\mathrm{EM},A}, \tag{3}$$

where m is the mass of the particle. Note that $f^i_{\mathrm{EM},A}$ should be expressed by the quantities in the TT coordinate.

Unlike a test particle, an elastic body consists of different parts, and their positions are better described by a displacement field, $\vec{\xi}(t, \vec{x})$, which quantifies the displacement of each part from the equilibrium position, $\vec{x}$. Without GWs and external forces, the evolution of the body is governed by

$$\rho\frac{\partial^2 \xi^i}{\partial t^2} = \frac{\partial \sigma^{ij}}{\partial x^j}, \tag{4}$$

where σ^{ij} is the stress tensor for a locally homogeneous and isotropic medium. The stress tensor can be calculated with

$$\sigma^{ij} = \lambda\delta^{ij}\frac{\partial \xi^k}{\partial x^k} + \mu\left(\frac{\partial \xi^i}{\partial x^j} + \frac{\partial \xi^j}{\partial x^i}\right), \tag{5}$$

where λ and μ are two Lamé constants, and μ is also called the "shear modulus." When GW is taken into account, Eq. (4) needs to be revised in two aspects (noted on p. 10 of Ha19). First, the meanings of $\vec{\xi}$ and $\vec{x}$ depend on the choice of coordinate system. In particular, when the TT coordinate is considered, $\vec{\xi}$ and $\vec{x}$ *do not* directly give the proper distance or proper length, but differ from them by a small quantity of the order of $\mathcal{O}(h)$. Second, even when all the displacement vanishes, i.e., $\vec{\xi}(t, \vec{x}) = 0$ in TT coordinate, a shear force can still be induced by the presence of GWs,

because GWs change the proper distance between different parts of the elastic body.

To account for these effects, a term should be added on the rhs of Eq. (4). As a result, Eq. (4), expressed in TT coordinate, becomes

$$\rho\frac{\partial^2\xi_A^i}{\partial t^2}=\frac{\partial}{\partial x_A^j}(\sigma_A^{ij}-\mu h^{ij}). \tag{6}$$

This equation first appeared in Dy69, which started from a field-theory approach, by writing down the interaction Lagrangian between GW and elastic body. Compared to Eq. (4), the additional μh^{ij} term comes from the shear force induced by GWs. Equation (6) also looks similar to Eq. (3). In fact, the rhs of Eq. (6) calculates precisely the total EM force $\vec{f}_{\mathrm{EM},A}$ per unit volume that is driving the elastic body away from the geodesic.

In the case of lunar GW detection, the GW wavelength is usually much longer than the size of the moon. Therefore, the gradient of h^{ij} over the entire body of the moon is small. We can approximate the last equation with

$$\rho\frac{\partial^2\xi_A^i}{\partial t^2}=\frac{\partial\sigma_A^{ij}}{\partial x_A^j}-\frac{\partial\mu}{\partial x_A^j}h^{ij}. \tag{6a}$$

B. Equations in the lab coordinate

Another coordinate system which is commonly used in textbooks and papers to describe the influence of GW is the "lab coordinate." It is also known as the "proper coordinate" because the spatial components are defined using the proper distance. The line element in this coordinate is

$$\mathrm{d}s^2=\eta_{\mu\nu}\mathrm{d}x_B^\mu\mathrm{d}x_B^\nu+\mathcal{O}(1)\times(R_{\mu l\nu m}x_B^l x_B^m)\mathrm{d}x_B^\mu\mathrm{d}x_B^\nu+\cdots, \tag{7}$$

where $R_{\mu l\nu m}$ is the Riemann curvature tensor, and we have used the subscript B to denote this coordinate. The factor of $\mathcal{O}(1)$ can be found in textbooks (e.g., Ref. [28]). Meanwhile, we have omitted the terms due to inertial acceleration and rotation of the lab frame because these effects due to the orbital motion and rotation of the moon appear at much lower frequencies than mHz. Given this simplification, the leading terms of the metrics in the coordinate systems A and B are exactly the same. In this way, the coordinates of the equilibrium positions have the same values, no matter which coordinate we choose.

In the lab coordinate B, the geodesic equation of a free, slow-moving particle can be written as

$$\frac{\mathrm{d}^2x_B^i}{\mathrm{d}t^2}=\frac{1}{2}\frac{\mathrm{d}^2h_j^i}{\mathrm{d}t^2}x_B^j. \tag{8}$$

The rhs is normally interpreted as a tidal force induced by GWs. Note that the components of the GW tensor in this equation can be made to appear identical to that in Eq. (6a) in the linear order, because there are sufficient residual freedom in two gauge choices [28], even though these two formulas are derived in different coordinate bases. With an additional EM force, $\vec{f}_{\mathrm{EM},B}$, the equation of motion becomes

$$m\frac{\mathrm{d}^2x_B^i}{\mathrm{d}t^2}=f_{\mathrm{EM},B}^i+\frac{1}{2}m\frac{\mathrm{d}^2h_j^i}{\mathrm{d}t^2}x_B^j. \tag{9}$$

One can compare it with Eq. (3) to see the consequence of choosing different coordinates.

To use Eq. (9) on elastic bodies, we notice that the first term on the rhs can be readily replaced by Eqs. (4) and (5), because they are already constructed using the proper distance. The second term does not depend on the property of an elastic body, and hence remains in the equation. Therefore, we derive

$$\rho\frac{\partial^2\xi_B^i}{\partial t^2}=\frac{\partial\sigma_B^{ij}}{\partial x_B^j}+\frac{1}{2}\rho\frac{\mathrm{d}^2h_j^i}{\mathrm{d}t^2}x_B^j. \tag{10}$$

Equations (6a) and (10) clearly show the difference caused by different coordinates. However, both equations describe the exact same dynamics. To see this equivalence, it is important to understand that the equilibrium positions, defined as zero-displacement position $\xi_{A/B}=0$, are physically different, even though numerically they may appear the same. More specifically, in coordinate B (lab frame) the equilibrium position maintains the same *proper* distance from the origin of the coordinate system. However, in coordinate A (TT frame), the equilibrium position changes its proper distance from the origin, while it is the coordinate distance (i.e., Δx_A^i) that is kept constant.

Because of this difference, the equilibrium point in coordinate B is accelerating with respect to the equilibrium point in A. The acceleration is $(d^2h_j^i/dt^2)x_{\mathrm{eq}}^j/2$ when measured in coordinate B, where x_{eq}^j is the coordinate of the equilibrium point. Notice that the values of x_{eq}^j in coordinate A and B differ by a small term of the order of $\mathcal{O}(h)$. Since the displacement fields $\vec{\xi}_A$ and $\vec{\xi}_B$ are defined relative to their respective equilibrium points, and by the rule of addition of acceleration, we have

$$\frac{\partial^2\xi_B^i}{\partial t^2}=\frac{\partial^2\xi_A^i}{\partial t^2}+\frac{1}{2}\frac{\mathrm{d}^2h_j^i}{\mathrm{d}t^2}x_{\mathrm{eq}}^j+\mathcal{O}(h^2). \tag{11}$$

The last term $\mathcal{O}(h^2)$ comes from a higher-order correction of the tidal force.

Finally, by combining Eqs. (6a), (10), and (11), we find that

$$\begin{aligned}\frac{\partial\sigma_A^{ij}}{\partial x_A^j}-\frac{\partial\mu}{\partial x_A^j}h^{ij}&=\frac{\partial\sigma_B^{ij}}{\partial x_B^j}+\frac{\rho}{2}\frac{\mathrm{d}^2h_j^i}{\mathrm{d}t^2}(x_B^j-x_{\mathrm{eq}}^j)\\&=\frac{\partial\sigma_B^{ij}}{\partial x_B^j}+\mathcal{O}(h^2).\end{aligned} \tag{12}$$

This equation can be considered as a projection of the same EM force onto two different sets of base vectors. In the following, we will omit the last term of the order of $\mathcal{O}(h^2)$.

C. Analytical solutions for a radially heterogeneous elastic sphere

A radially heterogeneous elastic sphere is a good first-order approximation of the real structure of the moon. Its surface response to GWs was first calculated analytically in BM83 using Eq. (6a), and later in Ma19 in more detail. Here we mainly follow the convention in Ma19 unless mentioned otherwise.

In Ma19, GW is described by a plane wave:

$$\mathbf{h} = \Re\{h_0 \epsilon_{ij} e^{i(\omega_g t - \vec{k}_g \cdot \vec{r})}\}, \tag{13}$$

where h_0 is the GW amplitude, ω_g is the GW angular frequency, and $\vec{k}_g = (0, 0, \omega_g/c)$ is the wave vector, which we assume to be pointing in the z direction, and

$$\epsilon_{ij} = \begin{bmatrix} 1 & 1 & 0 \\ 1 & -1 & 0 \\ 0 & 0 & 0 \end{bmatrix} \tag{14}$$

is the polarization tensor. This is identical to the $e = \lambda = \nu = 0$ case in Ma19. Notice that it is a special case in which the GW is linearly polarized. If it is in other polarization states, an $\mathcal{O}(1)$ modification should be made to the polarization-dependent part of the result [i.e., f^m in Eq. (15)]. We then neglect the $\vec{k}_g \cdot \vec{r}$ term in Eq. (13) because $\omega_g R/c \ll 1$, where R is the radius of the sphere.

Given the above GW, the analytical solution to Eq. (6a) is

$$\vec{\xi}^A_k(\theta, \varphi, t) = h_0 \vec{s}_k(\theta, \varphi) \Re\{\bar{g}_n(t)\} f^m \alpha^A_{2n}, \tag{15}$$

where $k = nlm$, $|m| \le l$, and for GWs only the spheroidal modes of $l = 2$ are excited [16,27]. The term $\vec{s}_k$ is the displacement eigenfunction of the spherical modes:

$$\begin{aligned} \vec{s}_k(\theta, \varphi) = {} & U_{2n}(R) \mathcal{Y}_{2m}(\theta, \varphi) \hat{e}_r \\ & + \frac{1}{\sqrt{6}} V_{2n}(R) \partial_\theta \mathcal{Y}_{2m}(\theta, \varphi) \hat{e}_\theta \\ & + \frac{1}{\sqrt{6}} V_{2n}(R) (\sin\theta)^{-1} \partial_\varphi \mathcal{Y}_{2m}(\theta, \varphi) \hat{e}_\varphi. \end{aligned} \tag{16}$$

The spherical coordinates here, θ and φ, mark the position on the surface of the sphere. The function $\bar{g}_n$ is called the source-time function, and it can be calculated with

$$\bar{g}_n(t) = \frac{e^{i\omega_g t}}{\omega_n^2 - \omega_g^2 + i\omega_n \omega_g / Q_n}. \tag{17}$$

Note that our $\bar{g}_n$ is slightly different from those in BM83 and Ma19 because of our choice of normalization, and we have verified it with our numerical calculations. The dependence on the wave vector $\vec{k}_g$ and polarization of GW is contained in

$$\begin{aligned} f^m &= f^m(e = \lambda = \nu = 0) \\ &= 4\sqrt{\frac{\pi}{15}} \times (\delta_{m,2} + \delta_{m,-2}). \end{aligned} \tag{18}$$

Finally, α^A_{2n} depends on the radial structure of the sphere,

$$\begin{aligned} \alpha^A_{2n} &= -\frac{\int_0^{R+} \frac{\partial \mu}{\partial r} (U_{2n}(r) + \frac{3}{\sqrt{6}} V_{2n}(r)) r^2 dr}{\int_0^R (U^2_{2n}(r) + V^2_{2n}(r)) \rho(r) r^2 dr} \\ &= \frac{\mu(R) R^2 (U_{2n}(R) + \frac{3}{\sqrt{6}} V_{2n}(R))}{\int_0^R (U^2_{2n}(r) + V^2_{2n}(r)) \rho(r) r^2 dr} \\ &\quad - \frac{\int_0^R \frac{\partial \mu}{\partial r} (U_{2n}(r) + \frac{3}{\sqrt{6}} V_{2n}(r)) r^2 dr}{\int_0^R (U^2_{2n}(r) + V^2_{2n}(r)) \rho(r) r^2 dr}. \end{aligned} \tag{19}$$

The upper-integration limit $R+$ in the first line means that the integration should be taken until the outer side of the surface. Notice that α_{2n} can be negative but it is real as long as $U_{2n}(r)$ and $V_{2n}(r)$ are real. The denominator in Eq. (19) comes from the normalization of $U^2_{2n} + V^2_{2n}$ in Ma19.

To derive the solution to Eq. (10), we find that the difference between Eqs. (6a) and (10) lies in the expression of the force density. Therefore, we can get the solution $\vec{\xi}^B_k(\theta, \varphi, t)$ by replacing $\partial\mu/\partial r$ in Eq. (19) with $\rho r \omega_g^2/2$, the tidal-force density in the frequency domain. Then we have

$$\alpha^B_{2n} = -\frac{\omega_g^2}{2} \frac{\int_0^R (U_{2n}(r) + \frac{3}{\sqrt{6}} V_{2n}(r)) \rho(r) r^3 dr}{\int_0^R (U^2_{2n}(r) + V^2_{2n}(r)) \rho(r) r^2 dr}. \tag{20}$$

Notice that this equation no longer contains the first term in Eq. (19), because the term comes from a discontinuity of the gradient of shear modulus at the surface. When the tidal-force density is involved, an integration over the surface does not lead to such a term.

D. Relation between the two analytical solutions

The solutions $\vec{\xi}^A_k$ and $\vec{\xi}^B_k$ derived above should, according to Eq. (11), satisfy the following relationship,

$$\vec{\xi}^A = \vec{\xi}^B - \frac{1}{2} \mathbf{h} \cdot \vec{R}, \tag{21}$$

where $\vec{R} = R(\sin\theta\cos\varphi, \sin\theta\sin\varphi, \cos\theta)$, and $\vec{\xi} \equiv \sum_{n,m} \vec{\xi}_k$.

In what follows, it is more instructive to write $\vec{\xi}$ in terms of its three spatial components,

$$\vec{\xi}(\theta,\varphi,t) = h_0 \cos(\omega_g t)\Big[T_r \sum_m f^m \mathcal{Y}_{2m}(\theta,\varphi)\hat{e}_r + T_h \sum_m f^m \partial_\theta \mathcal{Y}_{2m}(\theta,\varphi)\hat{e}_\theta + T_h \sum_m f^m \frac{\partial_\varphi \mathcal{Y}_{2m}(\theta,\varphi)}{\sin\theta}\hat{e}_\varphi\Big], \tag{22}$$

where we define the radial and horizontal response functions, respectively, as

$$T_r \equiv \sum_n U_{2n}\alpha_{2n}\Re\{\bar{g}_n(t)e^{-i\omega_g t}\} \tag{23}$$

and

$$T_h \equiv \sum_n \frac{V_{2n}}{\sqrt{6}}\alpha_{2n}\Re\{\bar{g}_n(t)e^{-i\omega_g t}\}. \tag{24}$$

We also find that (see Appendix-(A) for a proof)

$$\begin{aligned}
\frac{1}{2}\hat{e}_r\cdot\mathbf{h}\cdot\vec{R} &= \frac{R}{2}h_0\cos(\omega_g t)\sum_m \mathcal{Y}_{2m}(\theta,\varphi)f^m,\\
\frac{1}{2}\hat{e}_\theta\cdot\mathbf{h}\cdot\vec{R} &= \frac{R}{4}h_0\cos(\omega_g t)\sum_m \partial_\theta\mathcal{Y}_{2m}(\theta,\varphi)f^m,\\
\frac{1}{2}\hat{e}_\varphi\cdot\mathbf{h}\cdot\vec{R} &= \frac{R}{4}h_0\cos(\omega_g t)\sum_m \frac{\partial_\varphi\mathcal{Y}_{2m}(\theta,\varphi)}{\sin\theta}f^m.
\end{aligned} \tag{25}$$

Using the above equations, we can eliminate the common factors of Eq. (21). Finally, we find that

$$\begin{aligned}
T_r^A &= T_r^B - \frac{1}{2}R\\
T_h^A &= T_h^B - \frac{1}{4}R.
\end{aligned} \tag{26}$$

Notice that we have already used the following equation which comes from the definition of $\bar{g}_n(t)$, except for a small resonant frequency region $|\omega_g - \omega_n| < \omega_n/Q_n$:

$$\Re\{\bar{g}_n(t)e^{-i\omega_g t}\}\cos(\omega_g t) = \Re\{\bar{g}_n(t)\}. \tag{27}$$

We also clarify here that the different factors $1/2$ and $1/4$ in Eq. (26) come from the different factors on the rhs of Eq. (25), reflecting the behaviors of spherical harmonics. We will verify Eq. (26) in the next section by numerical calculations.

Several previous works tend to take T^B as the response function (e.g., [13,14]) and use it to infer the detectability of GWs. Here we would like to point out that T^B is not directly proportional to the readout of a seismometer, and hence should be used with caution. The reason is given in the next section.

III. NUMERICAL TEST AND APPLICATION

In this section, we first calculate the response functions for a simplified model, a homogeneous isotropic sphere, to verify our theory. Then we employ a more realistic lunar model to derive more realistic response functions. Based on these results, we discuss the implication for lunar GW detection. In the calculation, we use the MINEOS software package [33] to calculate the spheroidal eigenfunctions $U_{2n}(r)$ and $V_{2n}(r)$. We note that our V_{2n} is a factor of $\sqrt{6}$ smaller than that given by MINEOS because of a different normalization, according to the annotation in MINEOS.

A. Homogeneous isotropic sphere

We first consider a homogeneous isotropic sphere, with the radius $R = 1000$ km, density $\rho = 300\ \mathrm{kg\cdot m^{-3}}$, compressive wave speed $v_p = 8\ \mathrm{km\cdot s^{-1}}$, shear wave speed $v_s = 4\ \mathrm{km\cdot s^{-1}}$, and quality factor $Q = 1000$. These values qualitatively reflect the "averaged" properties of the moon. We choose two different numbers of layers in MINEOS, $N_L = 200$ and 2000. All the eigenfunctions for the first 400 normal modes (i.e., $0 \le n \le 400$) are calculated.

The resulting radial response functions are shown in Fig. 1. The plot shows that Eq. (26) works better at

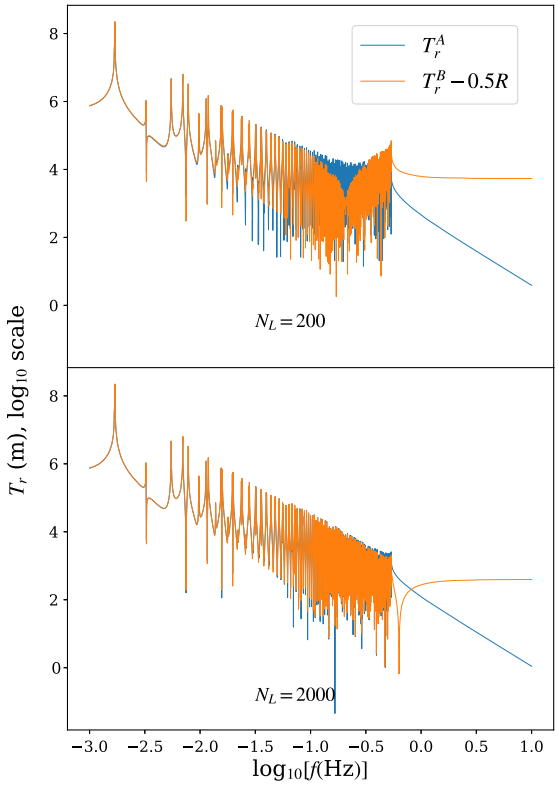

FIG. 1. Radial response functions $T_r(f)$ of a homogeneous isotropic sphere calculated using different numbers of layers N_L. Notice that both axes are in $\log_{10}$ scale. The results corresponding to the Dyson force (T_r^A) and tidal force ($T_r^B - 0.5R$) are shown in the same plot, for easier comparison.

lower frequencies, and also better when larger number of layers are used in the calculation. The improvement with respect to the number of layers can be understood as follows. When more layers are included, those eigenfunctions $U_{2n}(r)$ and $V_{2n}(r)$ with larger n can be more accurately calculated. Since larger n corresponds to higher eigenfrequencies ω_n, the response function at higher frequency also becomes more accurate. The mismatch at high frequency ($> 10^{-0.3}$ Hz) in the lower panel is mainly caused by our truncation of normal modes at $n = 400$. We also get similar results for the horizontal response function T_h, which is not shown here.

B. Real lunar model

Figure 2 shows the structure of our realistic lunar model. It was compiled from several published works [34–36] so that we could prepare a full input file for MINEOS. The model only has a homogeneous core, and has a low-velocity zone (LVZ) outside the core [37]. To increase the accuracy at high frequencies, we generate 28501 layers by interpolating with the original model data. The original and interpolated model files can be found in [38].

The most uncertain part is the Q value of the lunar core. We have run tests by changing $Q_{\rm core}$ between 200 and 5000. The results do not show characteristic difference, so the exact value of Q should not affect the main conclusions of this work. We choose $Q_{\rm core} = 1000$ in our model.

The radial and horizontal response functions derived for the interpolated model are shown in Fig. 3, panels (a) and (b). We have truncated the normal modes at $n = 400$. The value of the eigenfrequencies ω_n, quality factors Q_n, and response functions $T^A_{r/h}(f)$ can be found in [38]. At the frequencies lower than $10^{-0.6}$ Hz, we see a good agreement between the results derived from the Dyson force and the tidal force, which proves the validity of Eq. (26). The disagreement at higher frequencies, again, is caused by the artificial truncation of normal modes in the calculation.

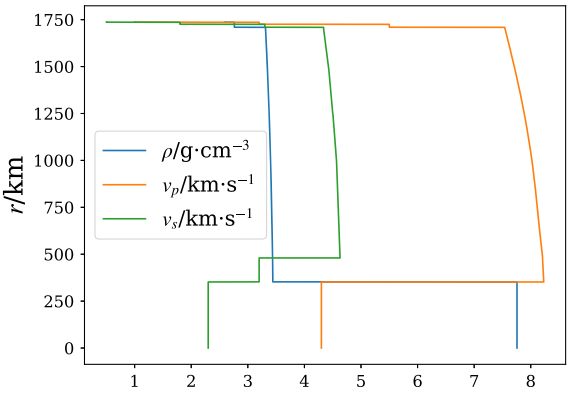

FIG. 2. Realistic lunar model used in this paper. The units are chosen so that three curves can be plotted using one x axis.

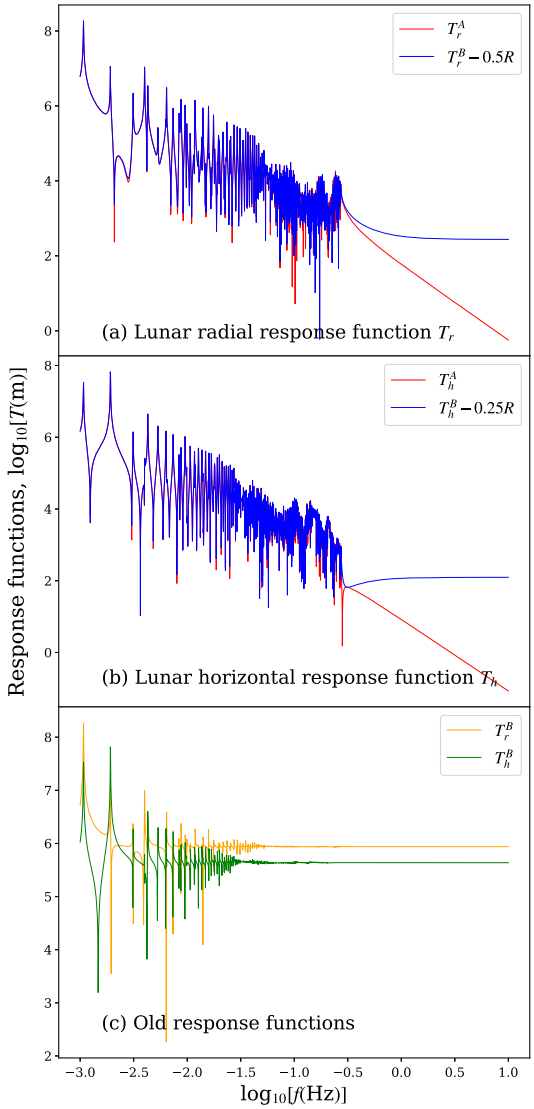

FIG. 3. Response functions for the realistic lunar model. (a) Radial response functions $T_r(f)$ derived from the Dyson force (A) and tidal force (B). (b) Horizontal response functions $T_h(f)$ for the two forces. (c) Old response functions T^B_r and T^B_h, which are derived following the method given in [13].

To compare with the response functions presented in earlier works, we also plot in Fig. 3(c) our T^B_r and T^B_h, but without subtracting, respectively, $0.5R$ and $0.25R$. The results recover those "old" response functions (e.g., presented in Fig. 1 of Ref. [13]). Comparing these old response functions with those new ones in Figs. 3(a) and 3(b), we find the difference at high frequencies, especially around 0.1 Hz, which was previously considered to be the sweet spot of a lunar GW detector.

C. Observables and detectability

To evaluate the detectability of GWs by future lunar seismology projects, we must first understand what is

observable. We emphasize here that it is the acceleration $\partial^2\xi^i_A/\partial t^2$, not $\partial^2\xi^i_B/\partial t^2$, that is a direct observable for a seismometer. Generally speaking, the former is measuring the *local* acceleration caused by EM forces, while the latter also counts for the tidal acceleration with respect to the center of the moon. The local acceleration is a quantity that an accelerometer, such as that installed in a lunar seismometer or gravimeter, can directly measure. The latter *tidal* acceleration, however, is not in simple proportion to the readout of the accelerometer. For example, consider two nearby test particles freely floating in a vacuum. When GWs pass by, the proper length between the two particles will vary, which induces a tidal acceleration. But, each particle actually follows its own geodesic motion (i.e., in free fall), so by the equivalence principle any small-sized instrumentation, such as an accelerometer, attached to either particle will give zero readout.

Given the sensitivity of a lunar seismometer, n_f (in unit of $\mathrm{m}\cdot\mathrm{s}^{-2}/\sqrt{\mathrm{Hz}}$), we can now use our response functions derived in coordinate A to estimate the minimal detectable characteristic strain of GW,

$$h_{n,r/h} = \frac{n_f}{(2\pi f)^{3/2} T^A_{r/h}}, \tag{28}$$

where the subscript r/h means radial or horizontal directions. For example, we consider two recently proposed lunar GW detectors, one based on the cryomagnetic design from the LGWA project [13] (hereafter "LGWA cryomagnetic") and the other operating at the moon surface temperature proposed by Beijing Normal University [14] (hereafter "BNU"). The resulting sensitivities of the instruments to GWs (i.e., $h_{n,r/h}$) are shown in Fig. 4. Most importantly, because of the updated response curves, our sensitivity curves are flat at $f < 0.1$ Hz, while those in the previous works show a V-shape centered at 0.1–1 Hz.

To understand the effect of the new response curves on GW observation, we also plot in Fig. 4 the characteristic strains of several IMBHBs and SMBHBs at different distances. For simplicity, the two black holes in the binary are considered to be equal, and the total mass is $m = 2\times10^6$, 2×10^5, or $2\times10^4 M_\odot$. We consider only circular orbits, so the characteristic strain can be calculated with

$$h_c(f) = 2f\tilde{h}(f), \tag{29}$$

where $\tilde{h}(f)$ is the Fourier transformation of the public PhenomA template [39]. The luminosity distance D_L is chosen to be 1, 0.1, and 0.02 Gpc, respectively, for the three total masses given above. It is a bit arbitrary, chosen for demonstration only. In any case, the characteristic strain is inversely proportional to D_L.

The signal-to-noise ratio (SNR) of a GW source is calculated according to the standard definition,

$$\mathrm{SNR}^2 = \int \mathrm{d}(\ln f)\frac{h_c^2}{h_n^2}. \tag{30}$$

Given the IMBHBs and SMBHBs specified above, the SNRs are 28.6,39.7, and 29.8 for LGWA cryomagnetic, and 0.42,0.86, and 1.02 for BNU. Although the SNRs for LGWA cryomagnetic are relatively high, the corresponding luminosity distances are significantly lower than the previous estimations [13,14] because here the response functions are updated using our own calculations. The lower D_L stresses the importance of improving the design of lunar seismometers to further suppress the instrument noise.

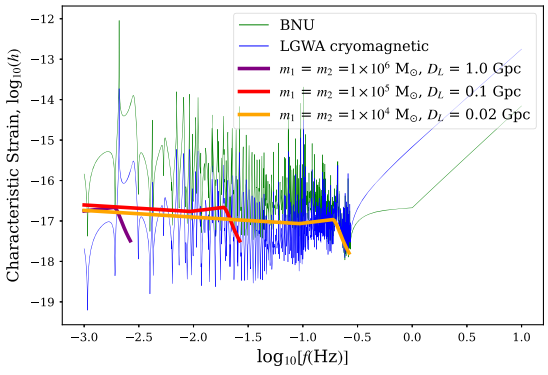

FIG. 4. GW characteristic strains for different instruments (thin lines) as well as representative astrophysical binary sources (thick lines).

IV. SUMMARY AND CONCLUSIONS

In this paper, we have revisited the theory of calculating the lunar response to GWs. We clarified an ambiguity which exists in the literature about two response functions derived from two viewpoints, one based on the Dyson force [Eq. (6a)] and the other from the ordinary tidal force [Eq. (10)]. We showed that the apparent difference between the two functions is caused by the choice of different coordinates.

Based on this understanding, we derived a concise and clear relationship between the two functions [see Eq. (26)]. We verified this analytical relationship by comparing the numerical response functions calculated using, respectively, the Dyson and tidal forces (see Fig. 3). A good agreement was found at lower frequencies. The deviation at higher frequencies can be attributed to (i) a truncation of the normal modes above a certain high value of n in our calculation and (ii) a limitation on the number of layers that we implemented in the lunar model.

The new response functions have a big impact on the detectability of GW sources by future lunar seismometers. As Fig. 4 has shown, the sensitivity to GWs given the current design of detectors flattens out between 10^{-3} and

0.1 Hz, making the detection of deci-Hertz GWs more challenging than previously thought. In particular, to detect IMBHBs and SMBHBs, which are important sources in the deci-Hertz GW band, it is essential to achieve in the 10^{-3}–0.1-Hz frequency band a sensitivity better than that of the cryomagntic detector design by the LGWA project. We believe our results will help shape up the scientific objectives of lunar GW observation, as well as provide important constraints on the design of lunar GW detectors.

Finally, we would like to point out that our response functions are derived based on the current normal-mode formulation of the dynamical equation of an elastic system in a GW field. There are important aspects of the lunar seismic response that are not captured by the current normal-mode model according to the data from the Apollo seismic observations [13,40]. Further studies on the lunar structure and lunar seismic response are urgently needed.

ACKNOWLEDGMENTS

This work is supported by the National Key Research and Development Program of China Grant Nos. 2021YFC2203002 and No. 2023YFC2205802, the Beijing Natural Science Foundation Grant No. 1242018, the Fundamental Research Funds for the Central Universities Grant No. 310432103, and the National Natural Science Foundation of China (NSFC) Grants No. 11991053, No. 12073005, No. 12021003, and No. 42325406. The authors would like to thank Yanbin Wang, Zijian Wang, and Junlang Li for many discussions. We thank Biao Yang for detailed information about the LVZ structure, and also thank Wuchuan Xu for his help in using the MINEOS package. Special thanks are due to our referee for many constructive suggestions.

APPENDIX: DETAILED DERIVATIONS OF EQ. (25)

Using the definitions of three base vectors:

$$\begin{aligned}\hat{e}_r &= (\sin\theta\cos\varphi, \sin\theta\sin\varphi, \cos\theta)\\ \hat{e}_\theta &= (\cos\theta\cos\varphi, \cos\theta\sin\varphi, -\sin\theta)\\ \hat{e}_\varphi &= (-\sin\varphi, \cos\varphi, 0),\end{aligned} \tag{A1}$$

we have

$$\begin{aligned}\hat{e}_r\cdot\epsilon\cdot\hat{e}_r &= \sin^2\theta(\sin 2\varphi + \cos 2\varphi)\\ \hat{e}_\theta\cdot\epsilon\cdot\hat{e}_r &= \sin\theta\cos\theta(\sin 2\varphi + \cos 2\varphi)\\ \hat{e}_\varphi\cdot\epsilon\cdot\hat{e}_r &= \sin\theta(-\sin 2\varphi + \cos 2\varphi).\end{aligned} \tag{A2}$$

According to Ma19, the definition of the real spherical harmonics leads to the following results:

$$\begin{aligned}\mathcal{Y}_{2,2}(\theta,\varphi) &= \frac{1}{4}\sqrt{\frac{15}{\pi}}\sin^2\theta\sin 2\varphi\\ \mathcal{Y}_{2,-2}(\theta,\varphi) &= \frac{1}{4}\sqrt{\frac{15}{\pi}}\sin^2\theta\cos 2\varphi.\end{aligned} \tag{A3}$$

Considering the definition of f^m, we have

$$\begin{aligned}\sum_m \mathcal{Y}_{2m}(\theta,\varphi)f^m &= \sin^2\theta(\sin 2\varphi + \cos 2\varphi)\\ \sum_m \partial_\theta\mathcal{Y}_{2m}(\theta,\varphi)f^m &= \sin 2\theta(\sin 2\varphi + \cos 2\varphi)\\ \sum_m \frac{\partial_\varphi\mathcal{Y}_{2m}(\theta,\varphi)}{\sin\theta}f^m &= 2\sin\theta(-\sin 2\varphi + \cos 2\varphi).\end{aligned} \tag{A4}$$

Thus, Eq. (25) has been proven by combining the above results.

[1] B. P. Abbott, R. Abbott, T. D. Abbott *et al.*, Observation of gravitational waves from a binary black hole merger, Phys. Rev. Lett. **116**, 061102 (2016).
[2] H. Xu, S. Chen, Y. Guo *et al.*, Searching for the nano-hertz stochastic gravitational wave background with the Chinese Pulsar Timing Array Data Release I, Res. Astron. Astrophys. **23**, 075024 (2023).
[3] EPTA, InPTA Collaborations, The second data release from the European Pulsar Timing Array. III. Search for gravitational wave signals, Astron. Astrophys. **678**, A50 (2023).
[4] G. Agazie, M. F. Alam, A. Anumarlapudi *et al.*, The NANOGrav 15 yr data set: Observations and timing of 68 millisecond pulsars, Astrophys. J. Lett. **951**, L9 (2023).
[5] D. J. Reardon, A. Zic, R. M. Shannon *et al.*, Search for an isotropic gravitational-wave background with the Parkes Pulsar Timing Array, Astrophys. J. Lett. **951**, L6 (2023).
[6] P. Amaro-Seoane, H. Audley, S. Babak *et al.*, Laser interferometer space antenna, arXiv:1702.00786.
[7] J. Luo, L.-S. Chen, H.-Z. Duan *et al.*, TianQin: A space-borne gravitational wave detector, Classical Quantum Gravity **33**, 035010 (2016).
[8] Z. Luo, Y. Wang, Y. Wu, W. Hu, and G. Jin, The Taiji program: A concise overview, Prog. Theor. Exp. Phys. **2021**, 05A108 (2021).
[9] M. Arca Sedda, C. P. L. Berry, K. Jani *et al.*, The missing link in gravitational-wave astronomy: Discoveries waiting

in the decihertz range, Classical Quantum Gravity **37**, 215011 (2020).
[10] S. Kawamura, M. Ando, N. Seto *et al.*, The Japanese space gravitational wave antenna: DECIGO, Classical Quantum Gravity **28**, 094011 (2011).
[11] S. Abend, B. Allard, I. Alonso *et al.*, Terrestrial very-long-baseline atom interferometry: Workshop summary, arXiv: 2310.08183.
[12] J. Weber, Gravitational waves, Phys. Today **21**, No. 4, 34 (1968).
[13] J. Harms, F. Ambrosino, L. Angelini *et al.*, Lunar gravitational-wave antenna, Astrophys. J. **910**, 1 (2021).
[14] J. Li, F. Liu, Y. Pan, Z. Wang, M. Cao, M. Wang, F. Zhang, J. Zhang, and Z.-H. Zhu, Detecting gravitational wave with an interferometric seismometer array on lunar nearside, Sci. China Phys. Mech. Astron. **66**, 109513 (2023).
[15] F. J. Dyson, Seismic response of the earth to a gravitational wave in the 1-Hz band, Astrophys. J. **156**, 529 (1969).
[16] A. Ben-Menahem, Excitation of the earth's eigenvibrations by gravitational radiation from astrophysical sources, Il Nuovo Cimento C **6**, 49 (1983).
[17] J. Majstorović, S. Rosat, and Y. Rogister, Earth's spheroidal motion induced by a gravitational wave in flat spacetime, Phys. Rev. D **100**, 044048 (2019).
[18] M. Coughlin and J. Harms, Constraining the gravitational wave energy density of the Universe using Earth's ring, Phys. Rev. D **90**, 042005 (2014).
[19] M. Coughlin and J. Harms, Constraining the gravitational-wave energy density of the Universe in the range 0.1 Hz to 1 Hz using the Apollo Seismic Array, Phys. Rev. D **90**, 102001 (2014).
[20] M. Coughlin and J. Harms, Upper limit on a stochastic background of gravitational waves from seismic measurements in the range 0.05–1 Hz, Phys. Rev. Lett. **112**, 101102 (2014).
[21] M. Kachelriess and M. P. Nødtvedt, Lunar response to gravitational waves, arXiv:2312.11665.
[22] M. Branchesi, M. Falanga, J. Harms *et al.*, Lunar gravitational-wave detection, Space Sci. Rev. **219**, 67 (2023).
[23] C. Z. Zhou and P. F. Michelson, Spherical resonant-mass gravitational wave detectors, Phys. Rev. D **51**, 2517 (1995).
[24] J. A. Lobo, What can we learn about gravitational wave physics with an elastic spherical antenna?, Phys. Rev. D **52**, 591 (1995).
[25] E. Coccia and V. Fafone, Coalescing binaries and spherical gravitational wave detectors, Phys. Lett. A **213**, 16 (1996).
[26] G. M. Harry, T. R. Stevenson, and H. J. Paik, Detectability of gravitational wave events by spherical resonant-mass antennas, Phys. Rev. D **54**, 2409 (1996).
[27] M. Bianchi, E. Coccia, C. N. Colacino, V. Fafone, and F. Fucito, Testing theories of gravity with a spherical gravitational wave detector, Classical Quantum Gravity **13**, 2865 (1996).
[28] C. W. Misner, K. S. Thorne, and J. A. Wheeler, *Gravitation* (W.H. Freeman and Company, San Francisco, 1973).
[29] M. Maggiore, Gravitational waves. Volume 1: Theory and experiments, Gen. Relativ. Gravit. **41**, 1667 (2009).
[30] I. M. Dozmorov, Theory of elastic solids in the gravitational internal system of reference (GISR), Sov. Phys. J. **19**, 741 (1976).
[31] I. M. Dozmorov, Interaction of a gravitational wave with an elastic body, Sov. Phys. J. **19**, 883 (1976).
[32] J. Harms, Terrestrial gravity fluctuations, Living Rev. Relativity **22**, 6 (2019).
[33] J. H. Woodhouse, in *Seismological Algorithms, Computational Methods and Computer Programs*, edited by D. J. Doornbos (Academic Press, London, 1988), pp. 321–370.
[34] R. C. Weber, P.-Y. Lin, E. J. Garnero, Q. Williams, and P. Lognonné, Seismic detection of the lunar core, Science **331**, 309 (2011).
[35] R. F. Garcia, J. Gagnepain-Beyneix, S. Chevrot, and P. Lognonné, Very preliminary reference Moon model, Phys. Earth Planet. Interiors **188**, 96 (2011).
[36] A. Briaud, C. Ganino, A. Fienga, A. Mémin, and N. Rambaux, The lunar solid inner core and the mantle overturn, Nature (London) **617**, 743 (2023).
[37] The parameters of the LVZ come from J. Zhang and his collaborators, while the related paper is still in preparation.
[38] https://github.com/StrelitziaHY/LunarResponse.
[39] P. Ajith, S. Babak, Y. Chen *et al.*, A phenomenological template family for black-hole coalescence waveforms, Classical Quantum Gravity **24**, S689 (2007).
[40] X. Zhang, L. Zhang, J. Zhang, and R. N. Mitchell, Strong heterogeneity in shallow lunar subsurface detected by Apollo Seismic Data, J. Geophys. Res. (Planets) **127**, e2022JE007222 (2022).